JACS
JOURNAL OF THE AMERICAN CHEMICAL SOCIETY

ARTICLE

pubs.acs.org/JACS

Structural Evolution of Iowa Mutant β-Amyloid Fibrils from Polymorphic to Homogeneous States under Repeated Seeded Growth

Wei Qiang, Wai-Ming Yau, and Robert Tycko*

Laboratory of Chemical Physics, National Institute of Diabetes and Digestive and Kidney Diseases, National Institutes of Health, Bethesda, Maryland 20892-0520, United States

Supporting Information

ABSTRACT: Structural variations in β-amyloid fibrils are potentially important to the toxicity of these fibrils in Alzheimer's disease (AD). We describe a repeated seeding protocol that selects a homogeneous fibril structure from a polymorphic initial state in the case of 40-residue β-amyloid fibrils with the Asp23-to-Asn, or Iowa, mutation (D23N-Aβ_{1-40}). We use thioflavin T (ThT) fluorescence, transmission electron microscopy (TEM), and solid-state nuclear magnetic resonance (NMR) to track the evolution of fibril structure through multiple generations under this protocol. The data show that (i) repeated seeding selectively amplifies a single D23N-Aβ_{1-40} fibril structure that can be a minor component of the initial polymorphic state; (ii) the final structure is highly sensitive to growth conditions, including pH, temperature, and agitation; (iii) although the initial state can include fibrils that contain both antiparallel and parallel β-sheets, the final structures contain only parallel β-sheets, suggesting that antiparallel β-sheet structures are thermodynamically and kinetically metastable. Additionally, our data demonstrate that ThT fluorescence enhancements, which are commonly used to monitor amyloid fibril formation, vary strongly with structural variations, even among fibrils comprised of the same polypeptide. Finally, we present a simple mathematical model that describes the structural evolution of fibril samples under repeated seeding.

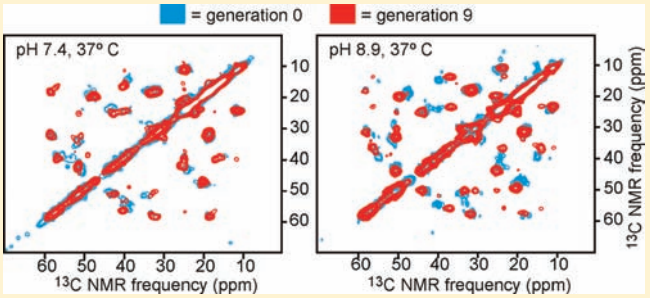

INTRODUCTION

Variations in the molecular structures of β-amyloid (Aβ) fibrils may be responsible for variations in the toxicity or patterns of deposition of these fibrils in Alzheimer's disease (AD).[1−3] Studies of structural variations in Aβ fibrils may then be important for understanding mechanisms of Aβ-induced neurodegeneration. Previous studies of wild-type 40-residue β-amyloid (WT-Aβ_{1-40}) fibrils revealed that fibrils grown with subtle differences in incubation conditions (e.g., the presence or absence of agitation during incubation) exhibit different morphological properties as well as differences in their underlying molecular structures.[1,4−7] Related observations have been reported for fibrils formed by other peptides and proteins.[8−11]

The existence of rare disease-associated mutations in the amyloid precursor protein provides evidence that Aβ aggregation leads to the pathogenesis of AD. Some of these mutations occur in the Aβ sequence itself, primarily in residues 21−23,[12] which form the beginning of a bend or loop that links β-strands in recent structural models for two distinct WT-Aβ_{1-40} polymorphs.[4,5,13] One such mutation is the Asp23-to-Asn (D23N) mutation, also called the Iowa mutation,[14] which causes neurodegeneration through cerebral amyloid angiopathy (CAA). In vitro, D23N-Aβ_{1-40} has been shown to form fibrils rapidly, without the characteristic lag period of WT-Aβ_{1-40} fibrillation kinetics.[15] Suprisingly, structural studies of D23N-Aβ_{1-40} fibrils by solid-state nuclear magnetic resonance (NMR) have shown[15] that the polymorphic mixture of structures, which typically forms when fibrils are grown from the monomeric peptide, contains not only fibrils with in-register parallel β-sheets, as found in WT-Aβ_{1-40} fibrils and numerous other examples of amyloid fibrils[10,16−19] and prion fibrils,[20,21] but also fibrils with antiparallel β-sheets, which had been found previously only in fibrils formed by relatively small peptides.[6,9,22] This finding raises the possibility that CAA caused by D23N-Aβ_{1-40} and other Aβ mutants may be associated specifically with antiparallel β-sheet structures.[15]

Given the pronounced polymorphism of D23N-Aβ_{1-40} fibrils and their association with neurodegenerative disease, it is important to investigate the dependence of D23N-Aβ_{1-40} fibril structure on growth conditions and to develop more detailed structural models for D23N-Aβ_{1-40} fibrils. Structural homogeneity is a prerequisite for detailed structural studies by solid-state NMR and other bulk measurements. Previous studies of WT-Aβ_{1-40} fibrils have shown that homogeneous samples can be created by multiple rounds, or generations, of seeded growth, starting from a polymorphic mixture.[4] Therefore, in the work described below, we have examined the dependence of D23N-Aβ_{1-40} fibril structure on variations in pH, temperature, and

Received: October 27, 2010
Published: February 28, 2011

agitation during fibrillation, and we have characterized the structural evolution that occurs when repeated rounds of seeded growth are performed. Using a combination of thioflavin T (ThT) fluorescence measurements (which report on growth kinetics and fibril structure), electron microscopy (which reveals morphological characteristics), and solid-state NMR (which distinguishes parallel from antiparallel β-sheets through $^{13}C-^{13}C$ dipolar recoupling measurements and reveals site-specific conformational variations through ^{13}C chemical shifts), we find that repeated seeded growth selects a single fibril structure from a polymorphic initial state, that the selected structure varies with growth conditions, and that antiparallel β-sheet structures are disfavored (both kinetically and thermodynamically) under conditions we have examined. Implications of these results are discussed below.

MATERIALS AND METHODS

Peptide Synthesis and Purification. D23N-Aβ_{1-40} was synthesized on an Applied Biosystems 433A peptide synthesizer with 9-fluorenylmethyloxycarbonyl (FMOC) chemistry (amino acid sequence NH_2-DAEFRHDSGY$_{10}$EVHHQKLVFF$_{20}$AENVGSNKGA$_{30}$ IIGLMVGGVV$_{40}$-COOH). Peptides were cleaved from the pre-loaded FMOC-Val-Wang resin (0.27 mequiv/g) using a mixture of TFA/phenol/H_2O/thioanisole/1,2-ethanedithiol with the volume ratio 82.5:5:5:5:2.5 for 1.75 h at ambient temperature. The crude product after cleavage was purified by reverse-phase HPLC on a preparative C3 reverse-phase column (Zorbax, Agilent Technologies) with a H_2O/acetonitrile gradient containing 1% acetic acid at ambient temperature. The molecular mass of the synthetic D23N-Aβ_{1-40} was verified, and purity greater than 95% was established by electrospray ionization and matrix-assisted laser-desorption-ionization time-of-flight mass spectrometry. For 2D solid-state ^{13}C NMR experiments, a D23N-Aβ_{1-40} sample was synthesized with uniform ^{13}C and ^{15}N labeling of Val18, Phe20, Ala30, Ile32, Leu34, Met35, and Gly38. For $^{13}C-^{13}C$ dipolar recoupling experiments, a sample was synthesized with ^{13}C labeling of the Val18 carbonyl site and the Ala21 methyl site, as well as ^{15}N labeling of the Phe20 amide site. Isotopically labeled amino acids were obtained from Cambridge Isotope Laboratories and Isotec/Sigma-Aldrich. Although ^{15}N labels were introduced, ^{15}N NMR measurements were not carried out. All peptides were lyophilized and stored at −25 °C after purification.

Fibril Formation and Sample Nomenclature. Four different fibrillation conditions were used, as follows: (A) pH 7.4, 37 °C, quiescent incubation; (B) pH 8.9, 37 °C, quiescent incubation; (C) pH 7.4, 37 °C, agitation during incubation; (D) pH 7.4, 24 °C, quiescent incubation. For different pH conditions, 10 mM phosphate buffer with 0.01% w/v NaN_3 was adjusted to either pH 7.4 or pH 8.9. Quiescent fibril growth at 37 °C was performed in an incubator (VWR model 1545) at 37 °C. Agitation was performed in an incubation shaker (New Brunswick Scientific model I2500) at 300 rpm and 37 °C.

Fibrils grown without seeding were considered generation 0. For these samples, lyophilized D23N-Aβ_{1-40} was first dissolved in dimethyl sulfoxide (DMSO) to a concentration of 5.8 mM, as determined by absorbance at 275 nm using the extinction coefficient for tyrosine of 1420 M^{-1} cm^{-1}. The DMSO solution was then diluted immediately into 10 mM phosphate buffer with the desired pH value, with thorough vortexing to ensure homogeneity of the solution. The final peptide concentration was approximately 100 μM. The peptide solution was incubated for approximately 5 days to form fibrils, as confirmed by both ThT fluorescence measurements and transmission electron microscope (TEM) images. Generation 0 samples formed under conditions A, B, C, and D are called Ag0, Bg0, Cg0, and Dg0.

Subsequent generations (with AgX representing generation X under growth condition A, for example) were prepared by dissolving lyophilized D23N-Aβ_{1-40} in DMSO, diluting to 25 μM peptide concentration in 10 mM phosphate at the desired pH, and "seeding" with an aliquot of the previous generation (starting with generation 0 to prepare generation 1). The aliquot volume was adjusted so that the seeds constituted approximately 9% of the total D23N-Aβ_{1-40} in the sample. Seeds were sonicated for 2 min with a probe sonicator (Branson model S-250A, 10% duty cycle and minimum power setting) before being added, so that fibrils in the seed solution were fragmented to lengths of 50−150 nm. Importantly, for growth conditions A, B, and D, the time interval between initial preparation of generation N-1 and initial preparation of generation N was fixed at 60 min (with the exception of generation 1, which was seeded with generation 0 fibrils that had been incubated for approximately 5 days). For growth condition C, the time between subsequent generations was 10 min for generations 1−7 and 5 min for generations 8−13. The shorter time intervals were required to avoid fibril precipitation (due to fragmentation and "clumping") under agitation in growth condition C, as discussed below.

Although time intervals between the initial preparation of subsequent generations were 5−60 min, each generation was incubated for 15−20 h in most experiments before electron microscopy or solid-state NMR experiments were performed. In certain cases noted below (Dg5s and Cg13s samples), fibril growth was arrested after 60 min by ultracentrifugation (Beckman Optima Max benchtop ultracentrifuge) at 435 000g for 60 min, freezing, and lyophilization.

As noted below, cross-seeding experiments were also performed in which Ag0 fibrils were used as the initial seeds for fibrils grown under condition B and vice versa. In these experiments, no conditions other than the identities of the generation 0 seeds were changed.

ThT Fluorescence. For each fluorescence intensity measurement, a 100 μL aliquot of the D23N-Aβ_{1-40} solution (25 μL for generation 0 samples, due to their higher concentration) was dispersed into 1.0 mL of 40 μM ThT solution in phosphate buffer at the relevant pH. Fluorescence emission spectra were recorded with excitation at 423 nm (monochromatic light-emitting diode source) and a 1 s integration time, using a StellarNet BLACK-Comet-TEC fluorescence spectrometer and a Hellma 119.004F-QS fluorescence cuvette. Reported fluorescence intensities are values at 490 nm, with error bars representing the total range of intensities in 10 consecutive spectra. Although fluorescence intensities are plotted in arbitrary units (a.u.), the units are the same in all measurements.

Electron Microscopy. Images were recorded with an FEI Morgagni TEM operating at 80 kV. For negatively stained images, a 10 μL drop of 25 μM fibril solution was absorbed for about 2 min on a glow-discharged carbon film, supported by lacey carbon on a 300 mesh copper TEM grid. After blotting, the grid was rinsed twice with deionized water, then stained with 10 μL of 3% uranyl acid for 40 s. The staining solution was then blotted, and the grid was dried in air before imaging. For measurements of mass-per-length (MPL), Ag9 and Bg9 fibrils were grown for only 60 min to avoid lateral assocation (i.e., "bundling" of individual fibrils into thicker structures). A 5 μL drop of 10 μM fibril solution was deposited on a grid with a thin carbon film (estimated 4 nm thickness). A 5 μL drop of tobacco mosaic virus (TMV) solution (roughly 0.5 mg/mL in pH 8 Tris buffer) was added, and the mixture was absorbed for 2 min. After blotting, the grid was rinsed once with deionized water, blotted, and dried in air. MPL values for individual fibril segments were obtained by quantification of intensities in dark-field images, using the tilted-beam TEM (TB-TEM) method described by Chen et al.[23] Dark-field images were recorded at 56 000× magnification with a 1.2° tilt of the electron beam and with careful adjustment of the electron beam to ensure uniform illumination of the image field and minimal beam damage to the sample. MPL histograms were generated from about 30 images, with intensity calibration in each image using an MPL value of 131 kDa/nm for TMV rods.

Solid-State NMR. For NMR measurements, D23N-Aβ_{1-40} fibrils were pelleted at 435 000*g* and 4 °C for 60 min. The pellet was frozen in liquid nitrogen and then lyophilized. The resulting powder was packed into a 3.2 mm thick-wall magic-angle spinning (MAS) rotor with additional Teflon spacers to keep the sample in the center of the NMR solenoid coil. All samples, except those used in PITHIRDS-CT measurements, were rehydrated in the MAS rotor with approximately 1 μL/mg deionized water. PITHIRDS-CT measurements were performed on dry lyophilized samples.

Solid-state NMR experiments were performed at 9.4 T (100.4 MHz ^{13}C NMR frequency) with a Varian InfinityPlus spectrometer and a Varian 3.2 mm MAS probe. MAS frequencies were 20.00 kHz. Radio-frequency (rf) field amplitudes during ^{1}H−^{13}C cross-polarization were 50 kHz for ^{13}C and 70 kHz for ^{1}H. For 2D solid-state ^{13}C NMR spectra, a 2.4 ms finite-pulse radio frequency-driven recoupling (fpRFDR) sequence with 15.0 μs ^{13}C π pulses was used during the mixing period;[24] two-pulse phase-modulated decoupling[25] with a 110 kHz ^{1}H rf field was used in the t_1 and t_2 periods. ^{1}H decoupling fields were 110 kHz during the dipolar recoupling period and 75 kHz during the acquisition period. ^{13}C chemical shifts are relative to tetramethylsilane, using the carbonyl signal of L-alanine powder at 177.95 ppm as an external reference.

For measurements of intermolecular ^{13}C−^{13}C dipole−dipole couplings, the PITHIRDS-CT technique was used as previously described.[26] Pulsed spin-locking was used during the acquisition period to enhance sensitivity.[27] The ^{13}C rf carrier frequency was placed on-resonance with the ^{13}C nuclei of interest (either V18 carbonyl or A21 methyl carbons). Numerical simulations verify that, under these experimental conditions and for relevant internuclear distances (greater than 6 Å), couplings between V18 carbonyl and A21 methyl carbons have a negligible effect on the experimental PITHIRDS-CT decay curves in Figure 5. These curves reflect V18−V18 or A21−A21 couplings, even though the D23N-Aβ_{1-40} sample was labeled at both V18 and A21.

Quantification of Residual Monomer Concentrations. D23N-Aβ_{1-40} solutions were subjected to ultracentrifugation at 435 000*g* for 60 min to pellet the fibrils. The supernatant was analyzed by fast protein liquid chromatography (FPLC), using an AKTApurifier 10 FPLC system and a Superdex Peptide 10/300 GL column. The peptide was eluted with a 50 mM phosphate buffer (150 mM NaCl, pH 7) in a time period of 30 min, detected by absorption at 254 nm. A linear working curve, which related [D23N-Aβ_{1-40}] to the time-integrated absorption, was plotted using a series of D23N-Aβ_{1-40} solutions with known concentrations in the 1−20 μM range. We estimate the minimum detectable concentration to be about 1 μM in a 1 mL volume.

RESULTS

Control Experiments. Seeded fibril growth is only effective when spontaneous nucleation of fibrils is negligible as compared to fibril growth by extension of seeds. At [D23N-Aβ_{1-40}] = 100 μM, previous measurements of growth kinetics by ThT fluorescence have shown the absence of a lag phase.[15] Therefore, we used [D23N-Aβ_{1-40}] = 25 μM as our initial peptide concentration and tested for de novo fibril growth under conditions A, B, C, and D (see Materials and Methods). As shown in Figure S1 of the Supporting Information, no increase in ThT fluorescence (i.e., negligible spontaneous nucleation) was observed over 60 min incubation periods, while data discussed below show that seeded growth occurs within 60 min. In addition, TEM images after 60 min showed no fibrils. We conclude that fibril growth in experiments described below is dominated by seeding. After longer incubation times, fibrils were observed by TEM at [D23N-Aβ_{1-40}] = 25 μM, with morphologies similar to those of the generation 0 fibrils at [D23N-Aβ_{1-40}] = 100 μM discussed below (see Figure S2 of the Supporting Information).

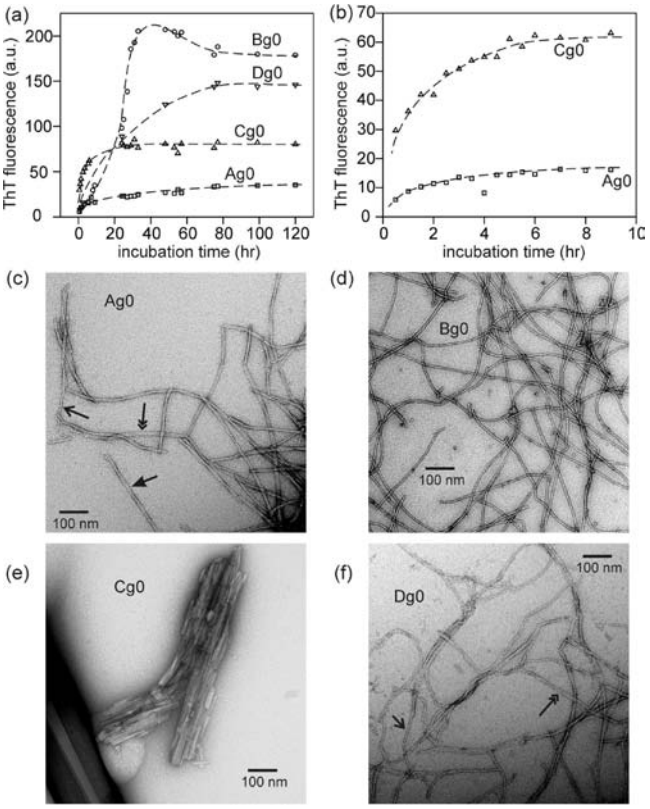

Figure 1. (a,b) D23N-Aβ_{1-40} fibril formation monitored by ThT fluorescence in unseeded experiments (i.e., generation 0) under experimental growth conditions A (□, pH 7.4, 37 °C), B (○, pH 8.9, 37 °C), C (Δ, pH 7.4, 37 °C, agitated), and D (∇, pH 7.4, 24 °C). (c−f) Negatively stained TEM images of the mature fibrils. Arrows with different styles in (c) and (f) indicate different morphologies.

The Initial D23N-Aβ_{1-40} Fibril Structure Depends on Growth Conditions. Figure 1a and b shows the dependences of ThT fluorescence on incubation time for generation 0 samples. For all growth conditions, the ThT fluorescence intensity reaches a plateau within 120 h. Large variations in asymptotic fluorescence intensities are observed, which must reflect variations in fibril structures and structural distributions. The nature of these variations cannot be determined, but ThT fluorescence is most likely sensitive to variations in conformational freedom and electrostatic environment in the dye binding site, which is not known definitively for any amyloid fibril.[28,29] Large variations in fluorescence intensity may not require large variations in fibril structure. Nonetheless, as shown below, these variations are highly reproducible, indicating that the structural variations are real.

The time scale for complete fibrillation also depends on growth conditions, with conditions A and C producing more rapid fibrillation than conditions B and D. Under condition C, rapid fibril formation is attributable to "self-seeding", in which shear forces from agitation of the D23N-Aβ_{1-40} solution break growing fibrils into shorter fragments, exposing more fibril ends and hence accelerating the addition of monomers to fibrils.[30] Similar effects of agitation have been observed for the wild-type Aβ fibrils.[11]

Figure 1c−f shows negatively stained TEM images for Ag0, Bg0, Cg0, and Dg0 fibrils after 120 h of incubation. Bg0 fibrils are primarily single filaments, without an apparent width modulation

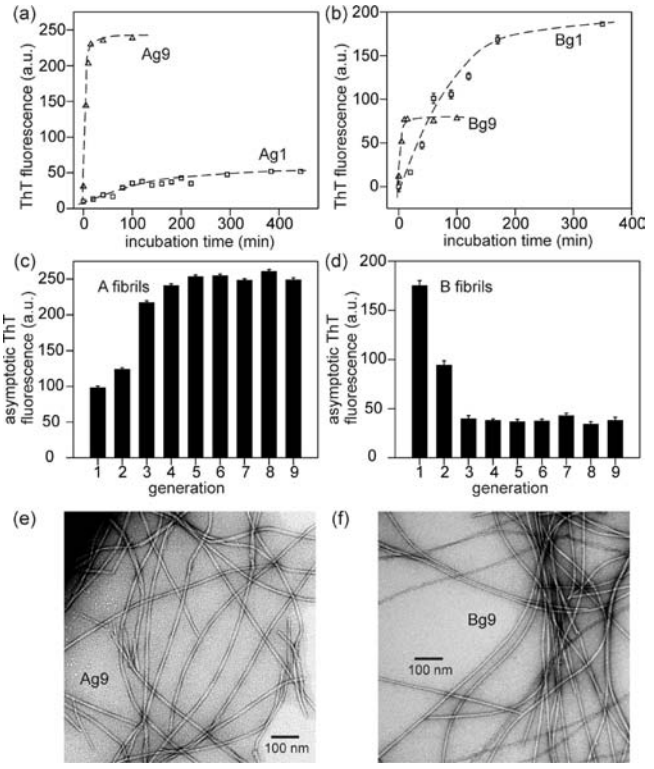

Figure 2. (a,b) Seeded D23N-Aβ_{1-40} fibril formation monitored by ThT fluorescence for generations 1 (□) and 9 (Δ) under growth conditions A (pH 7.4, 37 °C) and B (pH 8.9, 37 °C). (c,d) ThT fluorescence intensities for each generation of seeding after 48 h of fibril growth. (e,f) Negatively stained TEM images for fibrils Ag9 and Bg9, showing the final, homogeneous morphologies produced by repetitive seeding under conditions A and B with 60 min fibril growth in each generation.

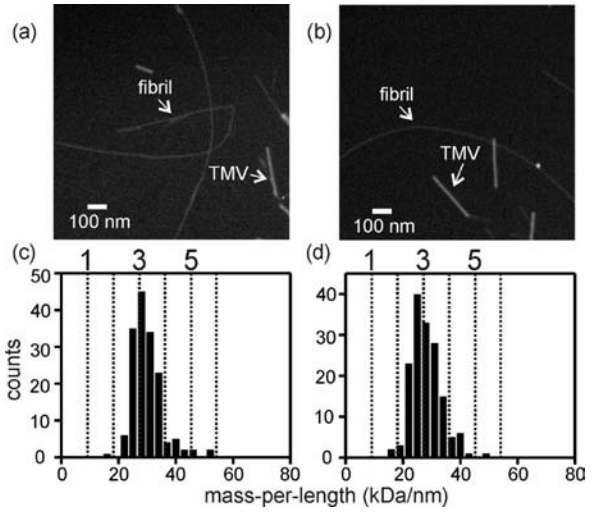

Figure 3. Dark-field TEM images and mass-per-length (MPL) histograms of unstained Ag9 (a,c) and Bg9 (b,d) fibrils, obtained with the tilted-beam technique described by Chen et al.[23] Tobacco mosaic virus (TMV) rods, codeposited with the D23N-Aβ_{1-40} fibrils, serve as internal MPL standards for intensities in each image. Dashed vertical lines in the MPL histograms indicate MPL values that ideally correspond to fibrils with 1−6 cross-β subunits, based on a molecular weight of 4.3 kDa for D23N-Aβ_{1-40} and a 0.48 nm intermolecular spacing within β-sheets. Histograms were generated from multiple dark-field images.

or twist, and without a propensity for self-association. Cg0 fibrils are relatively short, consistent with fragmentation by shear forces, and self-associate strongly. Ag0 and Dg0 are most similar morphologically, as both samples show long fibrils with distributions of self-association and twist.

Repeated Seeding Selects a Homogeneous Structure, Which Is pH-Dependent at 37 °C. Figure 2a and b shows ThT build-up curves for generation 1 and generation 9 fibrils under conditions A and B. In both cases, the generation 9 fibrils exhibit significantly faster fibrillation than do the generation 1 (or generation 0) fibrils, as well as significantly different asymptotic values of ThT fluorescence intensity. Figure 2c and d shows how the asymptotic fluorescence intensity increases with increasing generation for condition A and decreases with increasing generation for condition B. It appears that repeated seeding with a 60 min interval between generations favors fibril structures with rapid growth kinetics, that the selected structures at generation 9 are not the major structural component at generation 0, and that the selected structures are pH-dependent. Evolution toward structures with rapid kinetics can be understood if structurally distinct fibrils with distinct intrinsic extension rates are present in generation 0, and if the sonication process breaks all fibrils into fragments of similar length (see Discussion). The pH dependence of the selected structure (reflected in the different ThT fluorescence intensities from Ag9 and Bg9 fibrils) may then reflect pH dependences of fibril extension rates. Measurements of residual D23N-Aβ_{1-40} monomer concentrations after 60 min incubation periods also indicate more rapid fibril formation with increasing generation number, for conditions A, B, and D (see Figure S3 of the Supporting Information).

Reproducibility of the dependence of ThT fluorescence intensity on generation number was established by two independent trials of the repeated seeding experiments, for conditions A, B, C, and D (see Figure S4 of the Supporting Information).

TEM images of Ag9 and Bg9 fibrils in Figure 2e and f confirm that these fibrils are structurally distinct, but each is morphologically homogeneous. Ag9 fibrils exhibit an apparent width modulation, attributable to twist of the cross-β structure along the length of the fibril as in the WT-Aβ_{1-40} fibrils characterized by Paravastu et al.[4] Bg9 fibrils do not show such a modulation. Comparison with TEM images in Figure 1c and d shows that the Ag9 and Bg9 fibrils are not abundant in the corresponding generation 0 samples. Cross-seeding experiments, in which Ag0 seeds were used to initiate fibril growth under condition B and Bg0 seeds were used to initiate fibril growth under condition A, show that the asymptotic fibril morphology and ThT fluorescence intensity (at generation 9) are determined by growth conditions during the repeated seeding protocol, not by the conditions used to create generation 0 (see Figure S5 of the Supporting Information).

Figure 3 shows the results of MPL measurements on Ag9 and Bg9 fibrils, using the TB-TEM technique described by Chen et al.[23] For both fibrils, the MPL histogram peaks near 27 kDa/nm, the value expected for a cross-β structure comprised of three subunits. This interpretation follows from the 4.3 kDa molecular weight of D23N-Aβ_{1-40} and the 0.48 nm intermolecular spacing along the fibril axis in an ideal cross-β subunit (assuming one molecule per β-sheet spacing in each subunit).

To further characterize the structural evolution under our repeated seeding protocol, we recorded 2D solid-state ^{13}C NMR spectra of Ag1, Ag9, Bg1, and Bg9 fibrils formed from

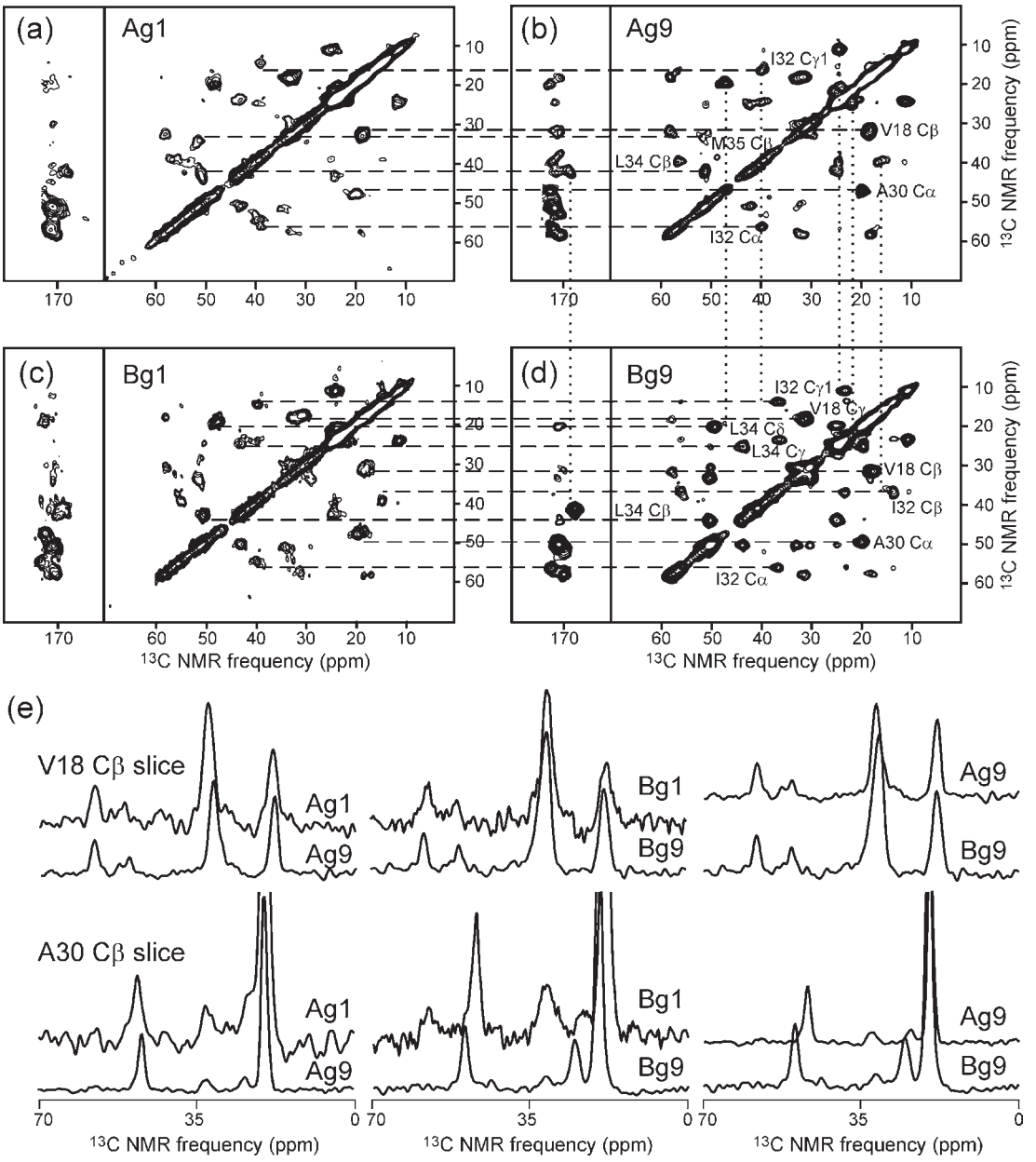

Figure 4. (a−d) 2D solid-state ^{13}C NMR spectra of Ag1, Ag9, Bg1, and Bg9 fibrils, prepared from D23N-Aβ_{1-40} with uniform ^{15}N and ^{13}C labeling of Val18, Phe20, Ala30, Ile32, Leu34, Met35, and Gly38. Dashed horizontal lines compare $^{13}C-^{13}C$ crosspeak positions for the generation 9 fibrils with crosspeak positions for the generation 1 fibrils. Dotted vertical lines compare crosspeak positions for Ag9 fibrils with crosspeaks positions for Bg9 fibrils. (e) 1D slices from the 2D spectra, permitting direct visualization of ^{13}C chemical shift changes and assessment of signal-to-noise.

D23N-Aβ_{1-40} with uniform ^{15}N and ^{13}C labeling of Val18, Phe20, Ala30, Ile32, Leu34, Met35, and Gly38. Figure 4a−d shows contour plots of the 2D spectra. Representative 1D slices are shown in Figure 4e. Under both growth conditions, repeated seeding produces significant changes in ^{13}C chemical shifts and significant reductions in NMR linewidths, indicating changes in the predominant fibril structures and reductions in heterogeneity. As examples, full-width-at-half-maximum (fwhm) linewidths for C_α/C_β crosspeaks of Ile32 are reduced from 2.1 ppm/2.4 ppm in Ag1 to 1.7 ppm/1.6 ppm in Ag9; C_α/C_β crosspeaks of Leu34 are reduced from 2.4 ppm/2.7 ppm in Ag1 to 1.3 ppm/1.9 ppm in Ag9; and C_α/C_β crosspeaks of Ala30 are reduced from 2.1 ppm/2.2 ppm in Ag1 to 1.5 ppm/1.7 ppm in Ag9. There is a 1.1 ppm upfield shift and a 50% line width reduction for C_α of Ala30. Side-chain sites of V18 and I32 show chemical shift differences greater than 1 ppm. Chemical shift differences between Bg1 and Bg9 samples are also striking. For example, C_α signals of both Ala30 and Ile32 show downfield shifts of roughly 2 ppm, and nearly all C_α/C_β are clearly sharper. The fwhm linewidths for C_α/C_β crosspeaks of Ile32 are reduced from 2.7 ppm/2.8 ppm in Bg1 to 1.5 ppm/1.8 ppm in Bg9; C_α/C_β crosspeaks of Leu34 are reduced from 2.0 ppm/2.5 ppm in Bg1 to 1.7 ppm/1.8 ppm in Bg9; and C_α/C_β crosspeaks of Ala30 are reduced from 2.0 ppm/2.4 ppm in Bg1 to 1.6 ppm/1.7 ppm in Bg9. 2D spectra of Ag9 and Bg9 are also significantly different from one another, with chemical shift differences greater than 1.5 ppm for many sites. ^{13}C chemical shifts for Ag9 and Bg9 fibrils (as well as Cg13 and Dg18 fibrils discussed below) are listed

dx.doi.org/10.1021/ja109679q | J. Am. Chem. Soc. 2011, 133, 4018–4029

Table 1. ^{13}C Chemical Shifts for Labeled Sites in D23N-Aβ_{1-40} Fibrils, along with Corresponding Random Coil (r.c.) Shifts[a]

	fibril sample	CO	C_α	C_β	C_γ	C_δ
Val18	Ag9	171.9	58.9	32.2	18.6	
	Bg9	170.3	58.4	32.4	18.8	
	Cg13	169.3	57.5	31.1	17.1	
	Dg18	170.0	57.8	31.6	17.5	
	r.c.	174.6	60.5	31.2	19.4, 18.6	
Phe20	Ag9		50.4	39.1		
	Bg9		52.4	40.4		
	Cg13		52.5	40.0		
	Dg18		53.0	40.2		
	r.c.		56.0	37.9		
Ala30	Ag9	172.7	47.6	20.4		
	Bg9	171.4	49.2	20.8		
	Cg13	171.7	47.1	19.3		
		170.8	48.5	20.0		
	Dg18	172.2	46.9	19.6		
	r.c.	176.1	50.8	17.4		
Ile32	Ag9	171.9	57.1	40.0	25.1, 17.1	11.8
	Bg9	172.7	56.9	37.5	24.0, 14.7	11.5
	Cg13	171.5	55.0	36.7	23.2, 14.0	10.6
	Dg18	171.6	56.2	38.5	23.2, 14.6	10.6
	r.c.	174.7	59.4	37.1	25.5, 15.7	11.2
Leu34	Ag9	171.7	51.7	42.8	25.6	22.3
	Bg9	170.9	51.0	44.6	25.4	20.4
	Cg13	170.0	50.1	43.4	24.3	20.1
				41.3		
	Dg18	170.8	50.9	42.6	23.5	20.0
	r.c.	175.9	53.4	40.7	25.2	23.2, 21.6
Met35	Ag9	171.3	51.6	33.6	31.2	
	Bg9	171.6	51.0	33.6	31.2	
	Cg13	170.2	50.1	33.6	28.1	
	Dg18	171.1	51.5	33.6	29.1	
	r.c.	174.6	53.7	31.2	30.3	
Gly38	Ag9	168.4	42.8			
	Bg9	168.0	42.8			
	Cg13	167.0	41.2			
		168.4				
	Dg18	168.1	41.6			
	r.c.	173.2	43.4			

[a] Shifts are in ppm relative to tetramethylsilane.

in Table 1, along with the relevant random coil shifts.[31] All labeled sites in Ag9 and Bg9 fibrils have ^{13}C shifts characteristic of β-strands (i.e., CO and C_α shifts upfield of random coil values; C_β shifts downfield of random coil values).

Previous solid-state NMR measurements on D23N-Aβ_{1-40} fibrils, grown under conditions that match those of our Ag0 samples, indicated the existence of antiparallel β-sheet structures within approximately 2/3 of the fibrils.[15] To address the important question of whether repeated seeded growth favors parallel or antiparallel β-sheet structures, we performed measurements of intermolecular ^{13}C−^{13}C dipole−dipole couplings using the PITHIRDS-CT dipolar recoupling technique,[26] which has also been used in previous studies of amyloid and prion fibrils.[3,4,21] In the present case, PITHIRDS-CT measurements were performed on Ag0, Ag9, Bg0, and Bg9 samples with ^{13}C labeling of the Val18 carbonyl site and the Ala21 methyl site, both of which are located in a β-strand. Data in Figure 5a show a reduction in the apparent average intermolecular distances among Val18 carbonyl carbons from approximately 6 Å in Ag0 and Bg0 samples to approximately 5 Å in Ag9 and Bg9 samples. Data in Figure 5b show intermolecular distances among Ala21 methyl carbons of approximately 5 Å in Ag9 and Bg9 samples, whereas Ag0 and Bg0 samples show rapidly decaying and slowly decaying signal components attributable to the coexistence of fibrils with intermolecular distances of approximately 5 Å and fibrils with intermolecular distances greater than 7 Å. Models for ideal antiparallel and parallel β-sheet structures in Figure 5c and d support the interpretation that both Ag0 and Bg0 contain mixtures of antiparallel and parallel β-sheet structures, but that Ag9 and Bg9 are almost entirely in-register parallel β-sheet structures. Prior data indicated that antiparallel β-sheets in D23N-Aβ_{1-40} fibrils have a hydrogen-bond registry that aligns Ala21 with Leu17.[15] This registry leads to nearest-neighbor intermolecular distances of approximately 6.1 Å for Val18 carbonyl carbons and approximately 10 Å for Ala21 methyl carbons, explaining the differences in generation 0 data between Figure 5a and b.

The Final D23N-Aβ_{1-40} Fibril Structures at 37 °C Are Both Kinetically and Thermodynamically Favored. Data in Figures 2−4 show that our repeated seeding protocol produces morphologically and structurally homogeneous fibril samples after nine generations, and that the final morphologies and molecular structures are different at pH 7.4 and pH 8.9. The final structures grow much more rapidly from seeds than do the majority of structures in the earliest generations (Figure 2a and b), but this fact alone does not imply that the final structures under this protocol are thermodynamically stable relative to the majority of structures in generation 0. To test for thermodynamic stability, we measured the time course of ThT fluorescence from 1:1 mixtures of mature generation 0 and mature generation 9 samples (Ag0:Ag9 and Bg0:Bg9). The mixtures were initially sonicated to create short fibril fragments that would reach equilibrium (by dissolution of less stable fibrils and growth of more stable fibrils) more rapidly than would longer fibrils. Data in Figure 6a and b show that ThT fluorescence intensities from these mixtures approach the values for the corresponding pure generation 9 samples, on time scales of 20−100 h. Thus, both Ag9 and Bg9 fibrils grow at the expense of other components of the generation 0 samples. Ag9 and Bg9 fibrils are thermodynamically favored over the majority of fibrils in the Ag0 and Bg0 samples, respectively.

TEM images obtained after the completion of ThT measurements (see Figure S6 of the Supporting Information) show relatively short, self-associated fibrils, making definitive identification of the predominant morphology difficult. The Ag0:Ag9 mixture contains fibrils with a visible twist, as in Figure 2e. The Bg0:Bg9 mixture does not contain identifiably twisted fibrils.

In related experiments, we sonicated Ag0, Bg0, Cg0, and Dg0 fibrils after 7 days of incubation and then monitored ThT fluorescence periodically for a 72 h period to detect structural changes (see Figure S7 of the Supporting Information). Relatively small changes in fluorescence intensities were observed for Ag0, Bg0, and Dg0, attributable to redistributions of populations among components that were present in these heterogeneous generation 0 samples. Fluorescence intensity increased for Ag0 and Dg0 and decreased for Bg0, consistent with trends observed

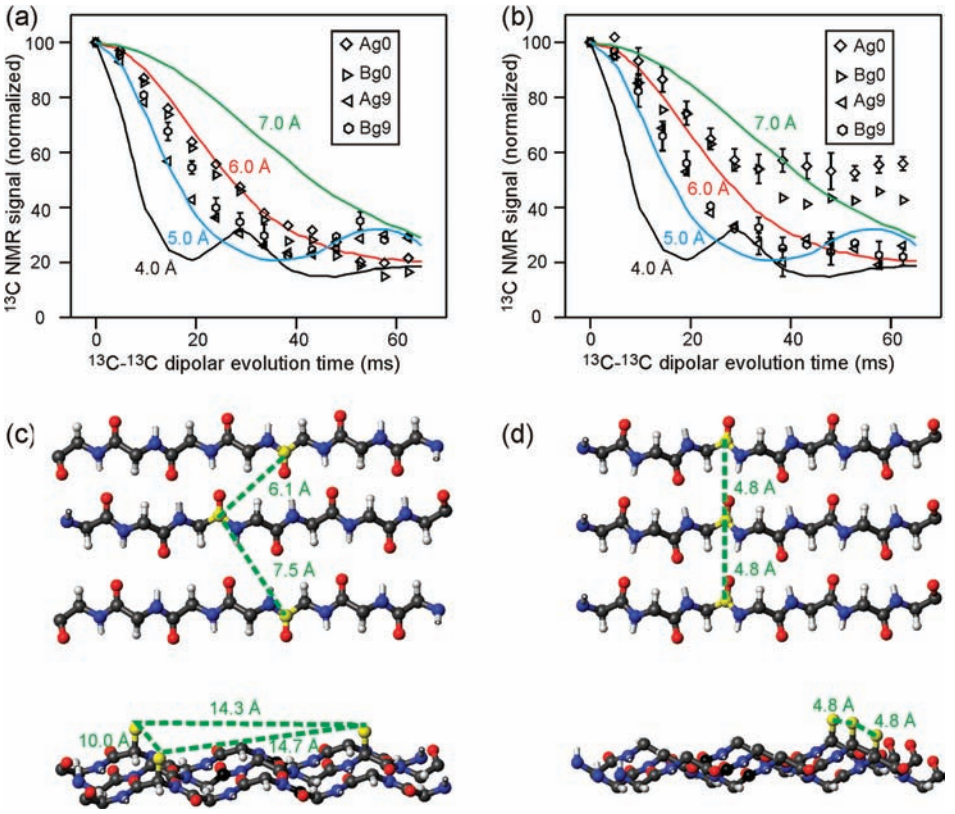

Figure 5. ^{13}C−^{13}C dipolar recoupling data for the Val18 carbonyl site (a) and Ala21 methyl site (b) in D23N-Aβ_{1-40} fibrils. Data are shown for unseeded (Ag0 and Bg0) and generation 9 (Ag9 and Bg9) fibrils. Simulated curves are for linear chains of ^{13}C nuclei with the indicated spacings. Molecular models created with MOLMOL[32] are shown for ideal antiparallel (c) and parallel (d) β-sheets. Intermolecular distances for Val18 carbonyl sites (upper models) and Ala21 methyl sites (lower models) are shown. The ^{13}C labels are yellow.

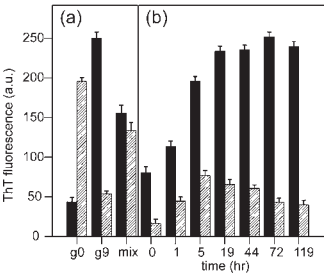

Figure 6. (a) ThT fluorescence intensities for generation 0 and generation 9 fibrils, and for 1:1 mixtures of the generation 0 and generation 9 fibrils. Data for fibrils grown under conditions A and B are represented by black and shaded bars, respectively. (b) Time-dependence of ThT fluorescence from the 1:1 mixtures after sonication at time 0.

in the repeated seeding data in Figures 2 and 7 (see below). Fluorescence intensity for Cg0 was constant, as might be expected because agitation during incubation results in short fibrils (see Figure 1e), which are then unaffected by sonication.

The Pathway to a Homogeneous D23N-Aβ_{1-40} Structure Is Temperature-Dependent at pH 7.4. ThT fluorescence build-up curves for Dg1, Dg5, Dg9, and Dg18 fibrils are shown in Figure 7a. These data clearly show a nonmonotonic dependence of the asymptotic fluorescence intensity on generation number, as well as a nonmonotonic dependence on incubation time for Dg5. Fluorescence intensities for generations 1−18 are shown in Figure 7b, measured both in the asymptotic limit (48 h incubation) and at an earlier incubation time (60 min). The complex behavior in Figure 7a and b suggests that one or more transient structural states with high ThT fluorescence enhancements arise during the incubation process in generations 3−7, and that the structures at long incubation times remain polymorphic through more than 10 generations before a homogeneous state is reached. The fibril structure that predominates in the asymptotic limit (after 16 generations) may remain a minor component until generation 11 or higher. The increasing ThT fluorescence intensity between generations 7 and 18 suggests that at least one transient state has appreciable population beyond generation 10. Negatively stained TEM images of Dg1, Dg5, Dg9, and Dg18 samples (see Figure S8 of the Supporting Information) support these suppositions. Dg18 fibrils do not tend to self-associate and have an apparently twisted morphology similar to that of Ag9 fibrils. The majority of fibrils in TEM images of Dg1, Dg5, and Dg9 do not have this appearance. Most Dg5 fibrils are relatively short and self-associate strongly. After 1 h of incubation, generation 5 fibrils (called Dg5s, with s indicating a "short" incubation period) are generally longer and less frequently self-associated. The transient, highly fluorescent state in generations 3−7 may then consist of unassociated, single fibrils, with self-association of these fibrils after long incubation periods having the effect of reducing the ThT fluorescence intensity by masking or altering the ThT binding site.

2D solid-state ^{13}C NMR spectra of Dg1, Dg5, Dg5s, Dg9, and Dg18 samples (Figure 7c−g) provide further support for these interpretations of the ThT and TEM data. The 2D spectrum of Dg1 shows relatively broad and weak crosspeaks, especially for

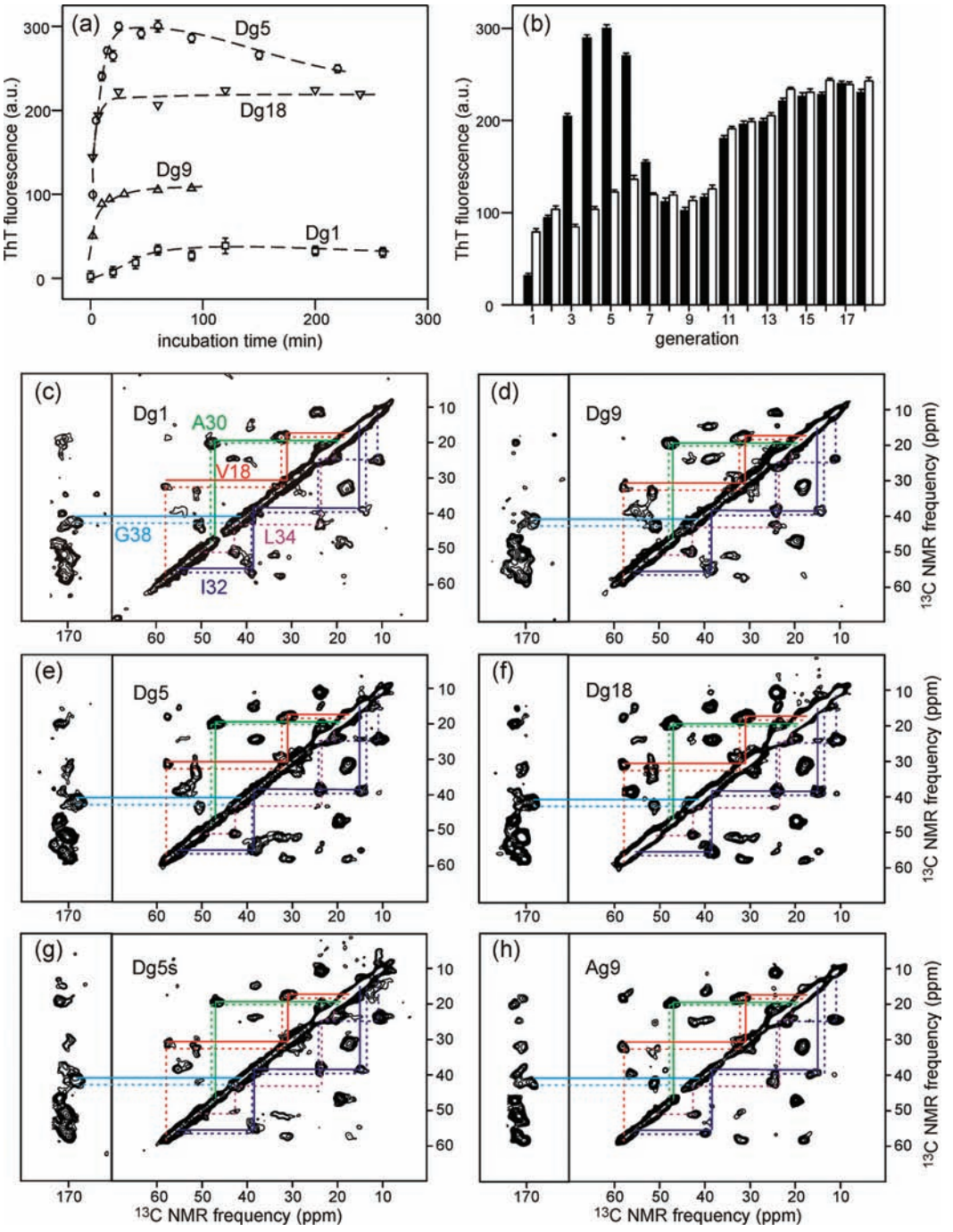

Figure 7. (a) Seeded D23N-Aβ_{1-40} fibril growth monitored by ThT fluorescence for generations 1 (□), 5 (○), 9 (Δ), and 18 (∇) under growth condition D (pH 7.4, 24 °C). (b) ThT fluorescence intensity after 1 h (black bars) and 48 h (white bars) for generations 1−18. (c−f) 2D solid-state ^{13}C NMR spectra of mature Dg1, Dg9, Dg5, and Dg18 fibril samples, respectively, prepared from D23N-Aβ_{1-40} with uniform ^{15}N and ^{13}C labeling of Val18, Phe20, Ala30, Ile32, Leu34, Met35, and Gly38. (g) 2D solid-state ^{13}C NMR spectrum of the Dg5s sample, which was collected by ultracentrifugation and lyophilized after only 60 min of fibril growth. (h) 2D solid-state ^{13}C NMR spectrum of the Ag9 sample. In all 2D spectra, color-coded dashed lines indicate the positions of intraresidue chemical shift assignment paths from the Dg1 spectrum. Solid lines indicate selected signals from the Dg18 spectrum that obviously differ from those in the Dg1 spectrum.

Leu34 (which shows distributions of C_α/C_β and C_β/C_γ crosspeak positions), Ile32 (for which $C_\beta/C_{\gamma1}$ and $C_\beta/C_{\gamma2}$ crosspeaks are weak), and A30 (which shows a broad C_α/C_β crosspeak). In contrast, the 2D spectrum of Dg18 (Figure 7f) shows substantially sharper and stronger crosspeaks for these sites, as well as many differences in ^{13}C chemical shifts. 2D spectra of Dg5 and Dg9 differ from one another and from 2D spectra of Dg1 and Dg18 (for example, in the region of C_α/C_β crosspeaks for Ile32 and Leu34), showing that 10 or more rounds of seeded growth are required to reach the final homogeneous structural state. 2D spectra of Dg5 and Dg5s are similar (exhibiting nearly the same ^{13}C chemical shifts, but with variations in crosspeak intensities),

dx.doi.org/10.1021/ja109679q | J. Am. Chem. Soc. 2011, 133, 4018–4029

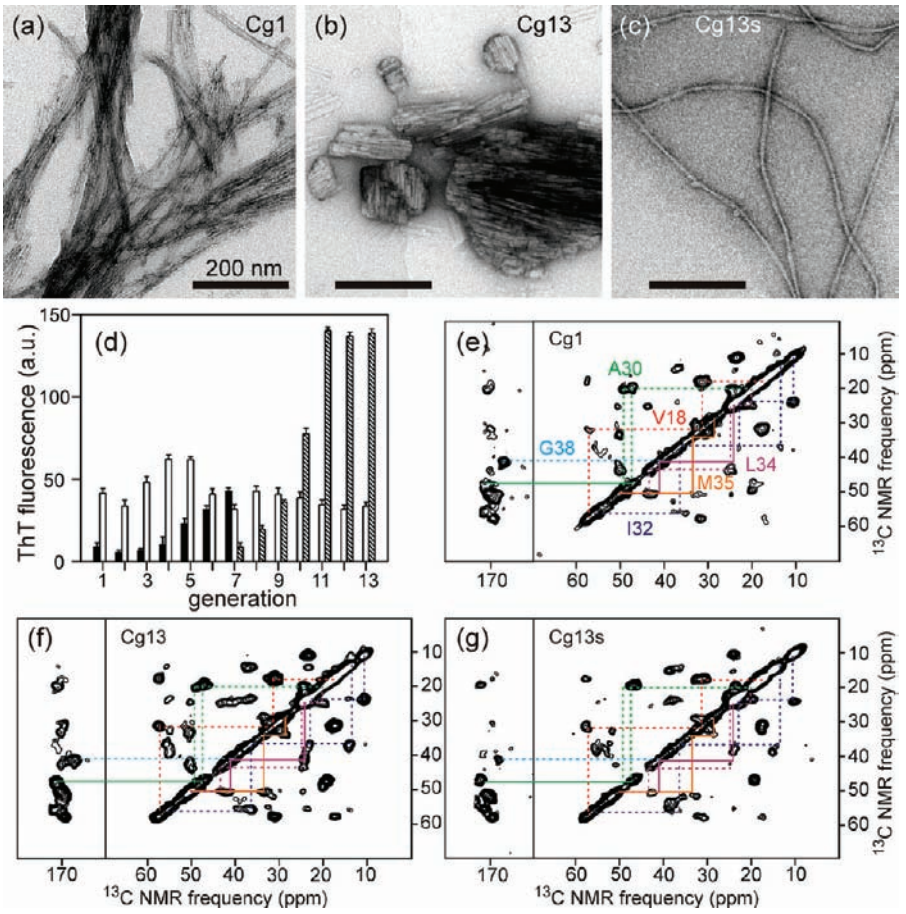

Figure 8. (a−c) Negatively stained TEM images of Cg1, Cg13, and Cg13s fibril samples. (d) ThT fluorescence intensity at 490 nm for seeded D23N-Aβ_{1-40} fibrils after 1 h (white bars), 5 min (shaded bars), and 10 min (black bars) of incubation under growth condition C (pH 7.4, 37 °C, agitated). (e−g) 2D spectra of Cg1, Cg13, and Cg13s fibrils, prepared from D23N-Aβ_{1-40} with uniform ^{15}N and ^{13}C labeling of Val18, Phe20, Ala30, Ile32, Leu34, Met35, and Gly38. The Cg13s sample was collected by ultracentrifugation and lyophilized after only 60 min of fibril growth. In all 2D spectra, color-coded dashed lines indicate the positions of intraresidue chemical shift assignment paths from the Cg1 spectrum. Solid lines indicate selected signals from the Cg13 spectrum that obviously differ from those in the Cg1 spectrum.

consistent with the idea that the nonmonotonic dependence of ThT fluorescence on incubation time in generation 5 is attributable to self-association of fibrils, rather than time-dependence of the structure within individual fibrils.

ThT fluorescence properties of Dg18 are nearly the same as those of Ag9, in that the fluorescence intensity increases to approximately 230 units within 10 min, suggesting that Dg18 and Ag9 (both formed at pH 7.4, but at 24 and 37 °C, respectively) might be the same structures. However, 2D spectra of Dg18 and Ag9 are not the same (Figure 7f and h), showing that Dg18 and Ag9 fibrils have somewhat different molecular structures.

Agitation Affects Both the Morphology and the Molecular Structures of D23N-Aβ_{1-40} Fibrils. In growth condition C, we applied agitation during incubation at pH 7.4 and 37 °C. When repeated seeding with 60 min growth periods between each generation was used, we observed that the fibril solutions changed from a clear and gel-like appearance during the first few minutes of incubation to a turbid appearance at later times, due to the formation of macroscopic "clumps" of fibril fragments during incubation under continuous agitation. We therefore used 10 min growth periods for generations 1−7 and 5 min growth periods for generations 8−13 under condition C. Figure 8a−c shows TEM images that illustrate the propensity of these fibrils to break and self-associate during incubation. The image of Cg13 fibrils (Figure 8b) was taken after overnight incubation, while the image of Cg13s fibrils (Figure 8c) was taken after only 5 min of incubation. In control experiments in which Cg13s fibrils were incubated quiescently for 48 h, fragmentation was not observed by TEM. Therefore, we attribute fragmentation to the shear forces that accompany agitation of the incubating solution.

Figure 8d shows that ThT fluorescence intensities increase with increasing generation number, provided that the fluorescence measurements are performed after 10 min (Cg1−Cg7) or 5 min (Cg7−Cg13). After generation 6, fluorescence intensities in each generation decrease significantly as incubation continues, apparently due to self-association and concomitant structural changes. Solid-state NMR spectra in Figure 8e and f show that repeated seeding produces significant changes in signals from A30, L34, and M35. Interestingly, spectra of Cg13 and Cg13s (Figure 8f and g) differ in the intensities of signals from I32, L34, and M35 and the ^{13}C chemical shifts of A30, I32, and G38. It appears that the molecular structure in Cg13 fibrils continues to evolve during incubation, as if the short growth periods between generations in these experiments lead to the selection and propagation of a

dx.doi.org/10.1021/ja109679q |J. Am. Chem. Soc. 2011, 133, 4018–4029

rapidly growing but metastable D23N-Aβ_{1-40} fibril structure (with high ThT fluorescence), which converts to a more stable structure (with lower ThT fluorescence) as incubation proceeds.

D23N-Aβ_{1-40} Fibrils Do Not Cross-Seed Wild-Type Aβ_{1-40}. We attempted to grow wild-type Aβ_{1-40} fibrils by adding sonicated fragments of Ag0, Ag9, Bg0, and Bg9 D23N-Aβ_{1-40} fibrils to solutions of monomeric wild-type Aβ_{1-40}. ThT fluorescence measurements showed no increase in fluorescence intensity for at least 60 min, indicating the absence of cross-seeding (see Figure S9 of the Supporting Information). Apparently, wild-type Aβ_{1-40} does not bind to or does not extend the ends of either antiparallel or parallel β-sheets in D23N-Aβ_{1-40} fibrils. The molecular basis for this incompatibility between D23N-Aβ_{1-40} and wild-type Aβ_{1-40} remains to be elucidated.

■ DISCUSSION

General Implications. Data presented above have several implications that may apply to amyloid fibrils generally, not only to D23N-Aβ_{1-40} fibrils: (i) Variations in growth conditions produce clear variations in morphology, as previously reported,[1,4−7] as well as variations in kinetics and in ThT fluorescence properties (Figure 1). ThT fluorescence intensity alone cannot be used to determine fibril quantities. (ii) Repeated seeding can selectively amplify a minor structural component of an initially polymorphic fibril sample, producing homogeneous samples with morphologies, ThT fluorescence properties, and molecular structures that depend on growth conditions (Figures 2, 4, and 7). When seeds are created by vigorous sonication, so that all fibrils are converted to fragments of approximately equal lengths, then differences in fibril extension rates are the main determinant of the structural evolution under repeated seeding. Fibril structures that grow most rapidly eventually predominate. (iii) In the case of D23N-Aβ_{1-40}, fibrils that become predominant after many generations also appear to be more thermodynamically stable (Figure 6). We do not know whether this is a general rule, but because thermodynamic stability is related to the ratio of "on" and "off" rate constants for the binding of peptide monomers to the ends of fibrils (i.e., the monomer concentration in equilibrium with structurally homogeneous fibrils equals this ratio if no other species exist), fibrils with high growth rates will tend to have high stability.

Earlier experiments by Petkova et al. showed that wild-type Aβ_{1-40} fibrils with distinct morphologies have distinct underlying molecular structures and that fibril morphologies and molecular structures are self-propagating in seeded growth.[1] Experiments on D23N-Aβ_{1-40} fibrils described above are complementary, showing how variations in fibril growth rates cause the relative populations of different fibril structures to evolve when a repeated seeding protocol is applied to a sample that is initially heterogeneous, eventually leading to a structurally and morphologically homogeneous sample after many generations.

Previous solid-state NMR studies of D23N-Aβ_{1-40} fibrils, grown quiescently and without seeding at pH 7.4 and 37 °C (i.e., condition A), revealed that a substantial fraction of the fibrils contain antiparallel β-sheets.[15] This was a surprising finding, because all previous studies of full-length wild-type Aβ fibrils[1,3,4,18,19] and other polypeptides longer than 15 residues[10,11,16,19−21] had found only in-register parallel β-sheets. Data in Figure 5 show that the antiparallel β-sheet component in polymorphic D23N-Aβ_{1-40} fibril samples is suppressed by repeated seeding, suggesting that fibrils with antiparallel β-sheet structures are inherently less stable than those with parallel β-sheet structures. Greater stability of parallel β-sheet structures is further supported by data in Figure 6. The observation of abundant fibrils with antiparallel β-sheets in unseeded samples (i.e., generation 0) may then indicate that spontaneous nucleation of these fibrils occurs more readily than nucleation of fibrils with the more stable parallel β-sheet structures.

Data in Figures 3 and 6 indicate that both Ag9 and Bg9 fibrils have molecular structures comprised of three cross-β units, with in-register parallel β-sheets. It is interesting that their ThT fluorescence intensities are quite different (Figure 2) despite these structural similarities. Solid-state NMR spectra in Figure 4 show large ^{13}C chemical shift differences for C_α of A30, for C_β and $C_{\gamma 2}$ of I32, and for C_β of L34. In existing structural models for WT-Aβ_{1-40} fibrils, these residues are located in the fibril core,[4,5] whereas recent computational studies suggest that ThT binding occurs in grooves on the fibril surface.[29] Structural variations that correlate with large variations in ThT fluorescence in our experiments are not limited to surface residues.

Several aspects of the results described above may have biomedical significance: (i) Structural heterogeneity of D23N-Aβ_{1-40} fibrils and pronounced differences in ThT fluorescence intensities suggest that amyloid-binding compounds for diagnostic imaging may preferentially target specific structures, which could be either useful or misleading. (ii) The dependence of fibril structures on growth conditions highlights the importance of identifying structures that develop in human brain tissue.[3] D23N-Aβ_{1-40} fibrils with antiparallel β-sheet structures may play a role in CAA,[15] but this possibility remains to be verified. Data presented above show that such fibrils are thermodynamically metastable under the conditions of our experiments, but nucleation of fibrils with antiparallel β-sheet structures is competitive with nucleation of fibrils with parallel β-sheet structures. (iii) Evolution of fibril structure analogous to results described above may be important in amyloid diseases if the proliferation of amyloid deposits throughout the affected tissue depends on fibril fragmentation (e.g., by phagocytosis) and subsequent transport or diffusion of fibril fragments. The development of specific strains in mammalian prion diseases and yeast prions may be influenced by similar processes.

Mathematical Model for Repeated Seeding. We conclude by describing a simple mathematical model that clarifies how variations in fibril extension rates can account for the experimentally observed evolution from a polymorphic to a homogeneous state under repeated seeded growth. We assume that the initial sample (i.e., generation 0) contains N distinct fibril structures with initial populations $f_q^{(0)}$ (measured as the concentration of peptide molecules contained in fibril structure q) and extension rates $r_q M(t)$, where $M(t)$ is the time-dependent concentration of peptide monomers. We further assume that, in the seeding protocol, all fibrils are broken into seeds containing ν monomers by sonication, a fraction η of these seeds are added to a fresh solution with peptide monomer concentration $M(0)$, and the solution is incubated for a time τ, producing fibril populations $f_q^{(k)}(\tau)$ in the kth generation. Ignoring dissociation of monomers from the ends of fibrils (which is much slower than the extension rates), spontaneous nucleation of fibrils, and fragmentation during the incubation periods, fibril populations during the

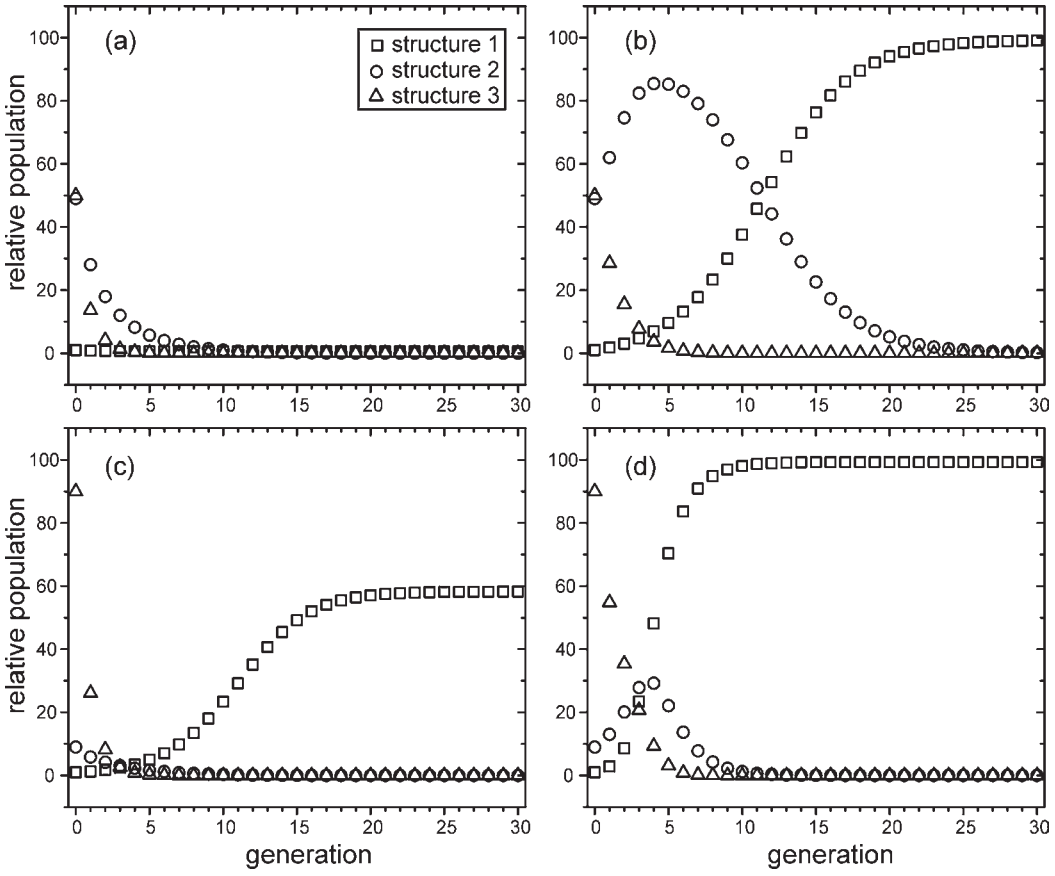

Figure 9. Numerical simulations of the evolution of fibril populations (i.e., values of $f_q^{(k)}(\tau)$ in eqs 1 and 2 of the text) under repeated seeding in a system with three distinct fibril structures. Populations in generation 0 (i.e., values of $f_q^{(0)}$) are 1, 49, and 50 (a,b) or 1, 9, and 90 (c,d). Growth rates (i.e., values of r_q) are 1.0, 0.7, and 0.3 (a,b) or 1.0, 0.5, and 0.2 (c,d). Incubation periods (i.e., values of τ) are 2 (a), 10 (b), 3 (c), or 10 (d). In all simulations, $\nu = 10$, $M(0) = 95$, and $\eta = 0.05$.

incubation period then satisfy the equations:

$$\frac{df_q^{(k+1)}(t)}{dt} = \frac{\eta f_q^{(k)}(\tau)}{\nu} r_q M(t) \quad (1a)$$

$$\frac{dM(t)}{dt} = -S^{(k)}M(t) \quad (1b)$$

$$S^{(k)} \equiv \sum_{q=1}^{N} \frac{\eta f_q^{(k)}(\tau)}{\nu} r_q \quad (1c)$$

which imply that fibril populations at the end of each incubation period in each generation are

$$f_q^{(k+1)}(\tau) = \eta f_q^{(k)}(\tau)\left\{1 + \frac{M(0)r_q}{\nu S^{(k)}}[1 - \exp(-S^{(k)}\tau)]\right\} \quad (2)$$

Equation 2 allows numerical simulations of the evolution of fibril populations to be performed. Examples of such simulations are shown in Figure 9, for a system with $N = 3$. If structure 1 is initially a minor component but has the largest extension rate (but only by a factor of 2), it becomes the predominant structure within a relatively small number of generations. Regardless of their initial populations, major components disappear after many generations if their extension rates are smaller. For certain choices of parameters, other components become predominant transiently, but later disappear (Figure 9b). The total fibril population decays toward 0 when $\eta(1 + M(0)r_q\tau/\nu) < 1$ for all q (Figure 9a). Otherwise, the minority component's population grows to an asymptotic value that satisfies the condition: $f_q = ((M(0)r_q)/(1 - \eta))[1 - \exp(-\eta f_q r_q \tau/\nu)]$.

Quantitative modeling of the experimental results in Figures 2c, d, 7b, and 8d is not possible (or is not unique) because we do not know the number of structural components in the generation 0 samples and the intrinsic ThT fluorescence intensities of the individual components. Nonetheless, it is worth noting that parameters such as those in Figure 9d result in behavior similar to that in Figure 2c, in that a nearly homogeneous sample is produced from a heterogeneous mixture within eight generations; parameters such as those in Figure 9b result in behavior similar to that in Figure 7b, in that an intermediate structure becomes predominant transiently, during generations 3−7, and the final structure becomes predominant after more than 10 generations.

■ ASSOCIATED CONTENT

Supporting Information. Figures showing the absence of spontaneous fibril nucleation within 60 min (Figure S1), the morphology of spontaneously nucleated fibrils at longer times (Figure S2), measurements of residual monomer concentrations (Figure S3), the reproducibility of ThT fluorescence data (Figure S4), results of Ag0/B and Bg0/A cross-seeding experiments

(Figure S5), TEM images of Ag0:Ag9 and Bg0:Bg9 mixtures (Figure S6), the time-dependence of ThT fluorescence from generation 0 fibrils after sonication (Figure S7), NMR and TEM data for fibrils grown under condition D (Figure S8), and the absence of cross-seeding between D23N-Aβ_{1-40} fibrils and wild-type Aβ_{1-40} (Figure S9). Complete author list for ref 2. This material is available free of charge via the Internet at http://pubs.acs.org.

AUTHOR INFORMATION

Corresponding Author
robertty@mail.nih.gov

ACKNOWLEDGMENT

This work was supported by the Intramural Research Program of the National Institute of Diabetes and Digestive and Kidney Diseases of the National Institutes of Health.

REFERENCES

(1) Petkova, A. T.; Leapman, R. D.; Guo, Z. H.; Yau, W. M.; Mattson, M. P.; Tycko, R. *Science* **2005**, *307*, 262.
(2) Meyer-Luehmann, M.; et al. *Science* **2006**, *313*, 1781.
(3) Paravastu, A. K.; Qahwash, I.; Leapman, R. D.; Meredith, S. C.; Tycko, R. *Proc. Natl. Acad. Sci. U.S.A.* **2009**, *106*, 7443.
(4) Paravastu, A. K.; Leapman, R. D.; Yau, W. M.; Tycko, R. *Proc. Natl. Acad. Sci. U.S.A.* **2008**, *105*, 18349.
(5) Petkova, A. T.; Yau, W. M.; Tycko, R. *Biochemistry* **2006**, *45*, 498.
(6) Petkova, A. T.; Buntkowsky, G.; Dyda, F.; Leapman, R. D.; Yau, W. M.; Tycko, R. *J. Mol. Biol.* **2004**, *335*, 247.
(7) Kodali, R.; Williams, A. D.; Chemuru, S.; Wetzel, R. *J. Mol. Biol.* **2010**, *401*, 503.
(8) (a) Pedersen, J. S.; Dikov, D.; Flink, J. L.; Hjuler, H. A.; Christiansen, G.; Otzen, D. E. *J. Mol. Biol.* **2006**, *355*, 501. (b) Debelouchina, G. T.; Platt, G. W.; Bayro, M. J.; Radford, S. E.; Griffin, R. G. *J. Am. Chem. Soc.* **2010**, *132*, 10414. (c) Toyama, B. H.; Kelly, M. J. S.; Gross, J. D.; Weissman, J. S. *Nature* **2007**, *449*, 233. (d) Heise, H.; Hoyer, W.; Becker, S.; Andronesi, O. C.; Riedel, D.; Baldus, M. *Proc. Natl. Acad. Sci. U.S.A.* **2005**, *102*, 15871. (e) Kodali, R.; Wetzel, R. *Curr. Opin. Struct. Biol.* **2007**, *17*, 48. (f) Ostapchenko, V. G.; Sawaya, M. R.; Makarava, N.; Savtchenko, R.; Nilsson, K. P. R.; Eisenberg, D.; Baskakov, I. V. *J. Mol. Biol.* **2010**, *400*, 908.
(9) Verel, R.; Tomka, I. T.; Bertozzi, C.; Cadalbert, R.; Kammerer, R. A.; Steinmetz, M. O.; Meier, B. H. *Angew. Chem., Int. Ed.* **2008**, *47*, 5842.
(10) Luca, S.; Yau, W. M.; Leapman, R.; Tycko, R. *Biochemistry* **2007**, *46*, 13505.
(11) Paravastu, A. K.; Petkova, A. T.; Tycko, R. *Biophys. J.* **2006**, *90*, 4618.
(12) (a) Tomiyama, T.; Nagata, T.; Shimada, H.; Teraoka, R.; Fukushima, A.; Kanemitsu, H.; Takuma, H.; Kuwano, R.; Imagawa, M.; Ataka, S.; Wada, Y.; Yoshioka, E.; Nishizaki, T.; Watanabe, Y.; Mori, H. *Ann. Neurol.* **2008**, *63*, 377. (b) Kumar-Singh, S.; Julliams, A.; Nuydens, R.; Ceuterick, C.; Labeur, C.; Serneels, S.; Vennekens, K.; Van Osta, P.; Geerts, H.; De Strooper, B.; Van Broeckhoven, C. *Neurobiol. Dis.* **2002**, *11*, 330. (c) Miravalle, L.; Tokuda, T.; Chiarle, R.; Giaccone, G.; Bugiani, O.; Tagliavini, F.; Frangione, B.; Ghiso, J. *J. Biol. Chem.* **2000**, *275*, 27110. (d) Melchor, J. P.; McVoy, L.; Van Nostrand, W. E. *J. Neurochem.* **2000**, *74*, 2209. (e) Davis, J.; VanNostrand, W. E. *Proc. Natl. Acad. Sci. U.S.A.* **1996**, *93*, 2996. Fraser, P. E.; Nguyen, J. T.; Inouye, H.; Surewicz, W. K.; Selkoe, D. J.; Podlisny, M. B.; Kirschner, D. A. *Biochemistry* **1992**, *31*, 10716.
(13) Sciarretta, K. L.; Gordon, D. J.; Petkova, A. T.; Tycko, R.; Meredith, S. C. *Biochemistry* **2005**, *44*, 6003.
(14) (a) Grabowski, T. J.; Cho, H. S.; Vonsattel, J. P. G.; Rebeck, G. W.; Greenberg, S. M. *Ann. Neurol.* **2001**, *49*, 697. (b) Van Nostrand, W. E.; Melchor, J. P.; Cho, H. S.; Greenberg, S. M.; Rebeck, G. W. *J. Biol. Chem.* **2001**, *276*, 32860.
(15) Tycko, R.; Sciarretta, K. L.; Orgel, J.; Meredith, S. C. *Biochemistry* **2009**, *48*, 6072.
(16) (a) Benzinger, T. L. S.; Gregory, D. M.; Burkoth, T. S.; Miller-Auer, H.; Lynn, D. G.; Botto, R. E.; Meredith, S. C. *Proc. Natl. Acad. Sci. U.S.A.* **1998**, *95*, 13407. (b) Der-Sarkissian, A.; Jao, C. C.; Chen, J.; Langen, R. *J. Biol. Chem.* **2003**, *278*, 37530. (c) Chan, J. C. C.; Oyler, N. A.; Yau, W. M.; Tycko, R. *Biochemistry* **2005**, *44*, 10669.
(17) (a) Antzutkin, O. N.; Balbach, J. J.; Leapman, R. D.; Rizzo, N. W.; Reed, J.; Tycko, R. *Proc. Natl. Acad. Sci. U.S.A.* **2000**, *97*, 13045. (b) Balbach, J. J.; Petkova, A. T.; Oyler, N. A.; Antzutkin, O. N.; Gordon, D. J.; Meredith, S. C.; Tycko, R. *Biophys. J.* **2002**, *83*, 1205.
(18) Torok, M.; Milton, S.; Kayed, R.; Wu, P.; McIntire, T.; Glabe, C. G.; Langen, R. *J. Biol. Chem.* **2002**, *277*, 40810.
(19) Antzutkin, O. N.; Leapman, R. D.; Balbach, J. J.; Tycko, R. *Biochemistry* **2002**, *41*, 15436.
(20) (a) Shewmaker, F.; Wickner, R. B.; Tycko, R. *Proc. Natl. Acad. Sci. U.S.A.* **2006**, *103*, 19754. (b) Baxa, U.; Wickner, R. B.; Steven, A. C.; Anderson, D. E.; Marekov, L. N.; Yau, W. M.; Tycko, R. *Biochemistry* **2007**, *46*, 13149. (c) Cobb, N. J.; Sonnichsen, F. D.; McHaourab, H.; Surewicz, W. K. *Proc. Natl. Acad. Sci. U.S.A.* **2007**, *104*, 18946.
(21) (a) Wickner, R. B.; Dyda, F.; Tycko, R. *Proc. Natl. Acad. Sci. U.S.A.* **2008**, *105*, 2403. (b) Tycko, R.; Savtchenko, R.; Ostapchenko, V. G.; Makarava, N.; Baskakov, I. V. *Biochemistry* **2010**, *49*, 9488.
(22) (a) Lansbury, P. T.; Costa, P. R.; Griffiths, J. M.; Simon, E. J.; Auger, M.; Halverson, K. J.; Kocisko, D. A.; Hendsch, Z. S.; Ashburn, T. T.; Spencer, R. G. S.; Tidor, B.; Griffin, R. G. *Nat. Struct. Biol.* **1995**, *2*, 990. (b) Balbach, J. J.; Ishii, Y.; Antzutkin, O. N.; Leapman, R. D.; Rizzo, N. W.; Dyda, F.; Reed, J.; Tycko, R. *Biochemistry* **2000**, *39*, 13748. (c) Sawaya, M. R.; Sambashivan, S.; Nelson, R.; Ivanova, M. I.; Sievers, S. A.; Apostol, M. I.; Thompson, M. J.; Balbirnie, M.; Wiltzius, J. J. W.; McFarlane, H. T.; Madsen, A. O.; Riekel, C.; Eisenberg, D. *Nature* **2007**, *447*, 453.
(23) Chen, B.; Thurber, K. R.; Shewmaker, F.; Wickner, R. B.; Tycko, R. *Proc. Natl. Acad. Sci. U.S.A.* **2009**, *106*, 14339.
(24) (a) Ishii, Y. *J. Chem. Phys.* **2001**, *114*, 8473. (b) Bennett, A. E.; Rienstra, C. M.; Griffiths, J. M.; Zhen, W. G.; Lansbury, P. T.; Griffin, R. G. *J. Chem. Phys.* **1998**, *108*, 9463.
(25) Bennett, A. E.; Rienstra, C. M.; Auger, M.; Lakshmi, K. V.; Griffin, R. G. *J. Chem. Phys.* **1995**, *103*, 6951.
(26) Tycko, R. *J. Chem. Phys.* **2007**, 126.
(27) Petkova, A. T.; Tycko, R. *J. Magn. Reson.* **2002**, *155*, 293.
(28) (a) Biancalana, M.; Makabe, K.; Koide, A.; Koide, S. *J. Mol. Biol.* **2009**, *385*, 1052. (b) Sabate, R.; Lascu, I.; Saupe, S. J. *J. Struct. Biol.* **2008**, *162*, 387. (c) Wu, C.; Wang, Z. X.; Lei, H. X.; Zhang, W.; Duan, Y. *J. Am. Chem. Soc.* **2007**, *129*, 1225.
(29) Wu, C.; Wang, Z. X.; Lei, H. X.; Duan, Y.; Bowers, M. T.; Shea, J. E. *J. Mol. Biol.* **2008**, *384*, 718.
(30) (a) Collins, S. R.; Douglass, A.; Vale, R. D.; Weissman, J. S. *PLoS Biol.* **2004**, *2*, 1582. (b) Knowles, T. P. J.; Waudby, C. A.; Devlin, G. L.; Cohen, S. I. A.; Aguzzi, A.; Vendruscolo, M.; Terentjev, E. M.; Welland, M. E.; Dobson, C. M. *Science* **2009**, *326*, 1533. (c) Smith, J. F.; Knowles, T. P. J.; Dobson, C. M.; MacPhee, C. E.; Welland, M. E. *Proc. Natl. Acad. Sci. U.S.A.* **2006**, *103*, 15806.
(31) Wishart, D. S.; Bigam, C. G.; Holm, A.; Hodges, R. S.; Sykes, B. D. *J. Biomol. NMR* **1995**, *5*, 67.
(32) Koradi, R.; Billeter, M.; Wuthrich, K. *J. Mol. Graphics* **1996**, *14*, 51.